A computational scheme of propagator method for moment equations to derive real-space electron transport coefficients in gas under crossed electric and magnetic fields

Hirotake Sugawara

***Abstract*—A numerical technique to calculate real-space electron transport coefficients in gas under crossed electric and magnetic fields ($\mathbf{E} \times \mathbf{B}$ fields) by propagator method was newly developed. Components of centroid drift velocity vector of an electron swarm and its diffusion coefficients defined in the $\mathbf{E}$, $\mathbf{B}$, and $\mathbf{E} \times \mathbf{B}$ directions were calculated by applying the propagator method stepwise to the zeroth-, first-, and second-order x, y, and z spatial moment equations derived from the Boltzmann equation. The results calculated for SF_6 at $N = 10^{22}$ $\mathbf{m}^{-3}$ in E/N and B/N ranges of 100–1000 Td and 100–1000 Hx, respectively, agreed with those obtained by Monte Carlo simulations with discrepancies of a few percent. The Hall deflection of the drift velocity vector and the direction dependency of the diffusion coefficients were appropriately reproduced. A relaxation scheme developed for quick convergence of the electron velocity distribution function was effective also in the relaxations of the first- and second-order spatial moment distribution functions. A prototype of the propagator method as a calculation scheme to derive a set of electron transport coefficients necessary for fluid model simulations of magnetized plasmas was established.**

***Index Terms*—crossed electric and magnetic fields, diffusion coefficient, drift velocity, electron swarm, electron velocity distribution, magnetized plasma, moment equation, propagator method**

I. Introduction

Propagator method (PM) is a numerical technique based on the Boltzmann equation (BE), and it is applicable to calculation of electron velocity distribution function (EVDF) in gases. The EVDF is one of the most fundamental properties of electrical discharges and plasmas because their macroscopic quantities such as physical and chemical reaction rates and electron transport coefficients are derived from the EVDF. Its field of use extends not only to gaseous plasmas [1] but also to liquids via plasma–liquid interactions [2]. Therefore, availability of reliable numerical tools to obtain the EVDF and associated electron transport coefficients from the electron–molecule interaction cross sections is of an important interest for investigators in the field of plasma analyses.

Manuscript received January 31, 2018; revised July 2, 2018; accepted August 9, 2018. Date of publication September 6, 2018. This work was supported by JSPS under KAKENHI Grant JP16K05626.

H. Sugawara is with Division of Electronics for Informatics, Graduate School of Information Science and Technology, Hokkaido University, Sapporo, 060-0814, Japan

e-mail: sugawara@ist.hokudai.ac.jp

Published source: IEEE Transactions on Plasma Science, vol. 47, no. 2, 1071-1082 (2019), DOI: 10.1109/TPS.2018.2866187

A brief history of the development of the PM in the research field of gas discharges and plasmas was presented in a recent paper [3]. The PM analyses of the EVDF started from those under static electric fields [4], [5]. After that, analyses by the PM in various simulation modes followed; e.g., those in the steady-state Townsend mode [6], [7], [8], [9], a radio-frequency (13.56 MHz) alternating electric field mode [10], [11], [12], and an impulse electric field mode [13]. The PM has also been applied to derivation of electron transport coefficients; e.g., drift velocities [14] and longitudinal and transverse diffusion coefficients [15], [16], [17]. The simulations in these investigations were all performed in the absence of magnetic field. It was recent that the PM was applied to the calculation of the EVDF under crossed electric and magnetic fields ($\mathbf{E} \times \mathbf{B}$ fields) [18], [19]. Enhancement of the PM technique as one of the practical computational methods such as Monte Carlo (MC) simulation and BE analysis would promote studies on electron transport in $\mathbf{E} \times \mathbf{B}$ fields, and that would contribute to investigations on magnetized plasmas utilized widely in etching and sputtering for material processing.

In the PM calculation for the EVDF, velocity space is partitioned into a number of cells. The number of electrons and relevant quantities associated with the cells are stored in arrays to calculate the EVDF. The intercellular electron transfers due to the electron acceleration by the applied external forces and electron scattering by gas molecules are calculated with operators called the propagators or Green's functions. By repeatedly applying the propagators to the EVDF, its relaxation is simulated.

The arrays required in the PM calculation may become huge corresponding to the resolution of the cell partition, especially in case the partition of velocity space is three-dimensional as is necessary under $\mathbf{E} \times \mathbf{B}$ fields. The requirement for the memory capacity and the computational power for many repetitive operations in the relaxation process had limited the use of the PM in the early decades despite the PM has merits that the PM does not require series expansion of the EVDF as done for multi-term BE analyses, temporal evolution of the EVDF and its equilibrium solution are both observable, and the PM calculation is free from statistical fluctuation as arises in MC simulations. However, today's enhanced computational resources allow us to carry out the PM simulations much more easily than before. Furthermore, higher performance would be realized by customized PM coding for advanced parallel

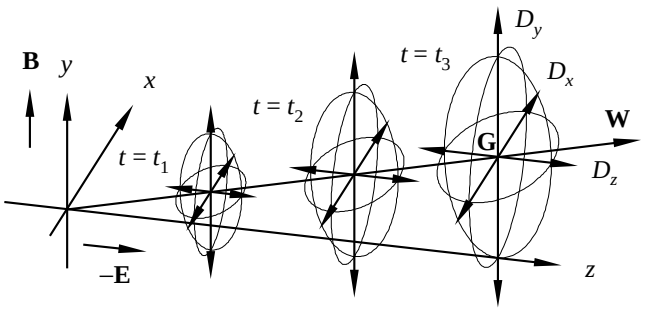

Fig. 1. Coordinate system and electron swarm development under $\mathbf{E} \times \mathbf{B}$ fields: drift to the $\mathbf{W}$ direction and diffusion in the x, y, and z directions. The Hall deflection occurs in the drift, and the diffusion relative to the centroid $\mathbf{G}$ is anisotropic.

processing facilities because a considerable part of the PM calculation is simple multiply-add operations.

In the present paper, the PM technique developed in the preceding work [18] for calculation of the EVDF under $\mathbf{E}$ and $\mathbf{B}$ fields crossed at a right angle is newly applied to the zeroth-, first- and second-order x, y, and z spatial moment equations derived from the BE in order to derive real-space electron transport coefficients as well. The components of centroid drift velocity vector and the diffusion coefficients defined along the $\mathbf{E}$, $\mathbf{B}$ and $\mathbf{E} \times \mathbf{B}$ directions are calculated as a benchmark, and they are compared with those obtained by MC simulations. These transport coefficients are known to be direction-dependent [20]. Thus, they are suitable as reference quantities for verification of the proposed PM scheme. The application of the PM to the spatial moment equations is one of the possible extensions of the preceding work [18] that achieved a fluctuation-free calculation of the EVDF and velocity-space electron transport coefficients under the $\mathbf{E} \times \mathbf{B}$ fields. The present effort for the real-space electron transport coefficients is a significant step in a framework to systematize the PM because the calculations of the drift velocity vector and direction-dependent diffusion coefficients are of a practical demand from fluid model simulations of plasmas. In addition, this effort is a demonstration to show the possibility of the PM for calculation of higher-order moment equations in a hierarchy. The scheme of the PM coupled with the moment equations is detailed and techniques for efficient numerical calculations are discussed.

II. Theory

A. Electric and magnetic fields

Let us assume the applied electric and magnetic fields, $\mathbf{E}$ and $\mathbf{B}$, to be static and uniform in boundary-free real space (x, y, z) as follows:

$$\mathbf{E} = (E_x, E_y, E_z) = (0, 0, -E) \quad (E > 0), \tag{1}$$

$$\mathbf{B} = (B_x, B_y, B_z) = (0, B, 0) \quad (B > 0). \tag{2}$$

The coordinate system and a schematic of direction-dependent electron swarm development under the $\mathbf{E} \times \mathbf{B}$ fields are illustrated in Fig. 1.

The electron acceleration $\mathbf{a} = (a_x, a_y, a_z)$ due to the Coulomb and Lorentz forces is written as

$$\mathbf{a} = \frac{d}{dt}\mathbf{v} = -\frac{e}{m}(\mathbf{E} + \mathbf{v} \times \mathbf{B}), \tag{3}$$

$$a_x = \frac{d}{dt}v_x = \frac{e}{m}v_z B = \omega v_z, \tag{4}$$

$$a_y = \frac{d}{dt}v_y = 0, \tag{5}$$

$$a_z = \frac{d}{dt}v_z = \frac{e}{m}(-v_x B + E) = -\omega\left(v_x - \frac{E}{B}\right), \tag{6}$$

where e and m are the electronic charge and mass, respectively, and $\omega = eB/m$ is the cyclotron angular frequency. When we consider a single electron motion in velocity space (v_x, v_y, v_z) under $\mathbf{a}$, the electron would draw a circular locus parallel to the $v_x v_z$-plane during its free flight [21] because the solutions of v_x and v_z obtained from (4) and (6) satisfy

$$\left(v_x - \frac{E}{B}\right)^2 + v_z^2 = \left(v_x|_{t=0} - \frac{E}{B}\right)^2 + (v_z|_{t=0})^2. \tag{7}$$

Here, E/B is the $\mathbf{E} \times \mathbf{B}$ drift velocity $v_{\mathbf{E}\times\mathbf{B}}$ under collisionless condition. This motion is interpreted as a rotational electron flow around an axis $(v_x, v_z) = (E/B, 0)$ parallel to the v_y-axis when we consider the EVDF of an electron swarm in velocity space.

B. Electron velocity and moment distribution functions

The real-space electron transport coefficients are derived from the spatial moments relative to the centroid $\mathbf{G}(t) = (G_x(t), G_y(t), G_z(t))$ of the electron swarm. Let us define the nth-order moment distribution functions in the laboratory and centroid systems, $m^{\mathrm{L}}_{n,r}(\mathbf{v}, t)$ and $m^{\mathrm{C}}_{n,r}(\mathbf{v}, t)$, respectively, where r represents one of the real-space coordinates x, y, and z.

From the electron distribution function $f(\mathbf{r}, \mathbf{v}, t)$ defined in phase space $(\mathbf{r}, \mathbf{v})$, we obtain the EVDF $f(\mathbf{v}, t)$ and $m^{\mathrm{L}}_{n,r}(\mathbf{v}, t)$ as follows:

$$f(\mathbf{v}, t) = \int_{\mathbf{r}} f(\mathbf{r}, \mathbf{v}, t) d\mathbf{r}, \tag{8}$$

$$m^{\mathrm{L}}_{n,r}(\mathbf{v}, t) = \int_{\mathbf{r}} r^n f(\mathbf{r}, \mathbf{v}, t) d\mathbf{r}. \tag{9}$$

Here, $m^{\mathrm{L}}_{0,x}(\mathbf{v}, t)$, $m^{\mathrm{L}}_{0,y}(\mathbf{v}, t)$, and $m^{\mathrm{L}}_{0,z}(\mathbf{v}, t)$ are all identical to $f(\mathbf{v}, t)$. $m^{\mathrm{C}}_{n,r}(\mathbf{v}, t)$ is derived as

$$n_{\mathrm{e}}(t) = \int_{\mathbf{r}}\int_{\mathbf{v}} f(\mathbf{r}, \mathbf{v}, t) d\mathbf{r} d\mathbf{v} = \int_{\mathbf{v}} f(\mathbf{v}, t) d\mathbf{v}, \tag{10}$$

$$G_r(t) = \frac{1}{n_{\mathrm{e}}(t)}\int_{\mathbf{r}}\int_{\mathbf{v}} r f(\mathbf{r}, \mathbf{v}, t) d\mathbf{r} d\mathbf{v} = \frac{1}{n_{\mathrm{e}}(t)}\int_{\mathbf{v}} m^{\mathrm{L}}_{1,r}(\mathbf{v}, t) d\mathbf{v}, \tag{11}$$

$$m^{\mathrm{C}}_{n,r}(\mathbf{v}, t) = \int_{\mathbf{r}} [r - G_r(t)]^n f(\mathbf{r}, \mathbf{v}, t) d\mathbf{r}, \tag{12}$$

where $n_{\rm e}(t)$ is the number of electrons in the electron swarm. $m^{\rm L}_{n,r}(\mathbf{v},t)$ and $m^{\rm C}_{n,r}(\mathbf{v},t)$ are convertible each other using $G_r(t)$ via (12). Their relations up to $n=2$ are

$$m^{\rm C}_{0,r}(\mathbf{v},t) = m^{\rm L}_{0,r}(\mathbf{v},t) = f(\mathbf{v},t), \quad (13)$$

$$m^{\rm C}_{1,r}(\mathbf{v},t) = m^{\rm L}_{1,r}(\mathbf{v},t) - G_r(t) m^{\rm L}_{0,r}(\mathbf{v},t), \quad (14)$$

$$m^{\rm C}_{2,r}(\mathbf{v},t) = m^{\rm L}_{2,r}(\mathbf{v},t) - 2G_r(t) m^{\rm L}_{1,r}(\mathbf{v},t) + [G_r(t)]^2 m^{\rm L}_{0,r}(\mathbf{v},t). \quad (15)$$

$m^{\rm L}_{n,r}(\mathbf{v},t)$ and $m^{\rm C}_{n,r}(\mathbf{v},t)$ have such quantities that $m^{\rm L}_{n,r}(\mathbf{v},t)d\mathbf{v}$ and $m^{\rm C}_{n,r}(\mathbf{v},t)d\mathbf{v}$ are the total amounts of the nth-order r-direction moments of electrons within a region $d\mathbf{v}$ at $\mathbf{v}$. They are sub-ensembles to obtain the electron population $n_{\rm e}(t)$ ($n=0$), the average position or the centroid $\mathbf{G}(t)$ ($n=1$), and the variance ($n=2$) of the electron swarm with respect to the r direction. The temporal variation of the average position is the centroid drift velocity, and that of the variance gives the diffusion coefficient in the r direction as shown in the next subsection.

C. Electron transport coefficients

Primary electron transport coefficients of the electron swarm to be derived by the present PM in this paper are the mean electron energy $\bar{\varepsilon}$, the effective ionization frequency $\bar{\nu}_{\rm ion} = \nu_{\rm ion} - \nu_{\rm att}$ (where $\nu_{\rm ion}$ and $\nu_{\rm att}$ are the ionization and attachment frequencies), the centroid drift velocity $\mathbf{W} = (W_x, W_y, W_z) = (W_{\mathbf{E}\times\mathbf{B}}, W_{\mathbf{B}}, W_{\mathbf{E}})$, and the diffusion coefficients $D_x = D_{\mathbf{E}\times\mathbf{B}}$, $D_y = D_{\mathbf{B}}$, and $D_z = D_{\mathbf{E}}$ defined along the x, y, and z directions, respectively. They are typical coefficients required in fluid model simulations. Here, $\mathbf{W}$ may have different values from the average electron velocity $\mathbf{V} = (V_x, V_y, V_z) = (V_{\mathbf{E}\times\mathbf{B}}, V_{\mathbf{B}}, V_{\mathbf{E}})$ when the electron swarm is non-conservative in the presence of ionization and/or electron attachment [14], [22]. While they are time-dependent during the relaxation process of the electron swarm, we assume that they eventually reach constant values in drift equilibrium. Let us denote their time-dependent values with '(t)', and '(t)' is omitted for the time-invariant values when they are distinguished hereafter.

$\bar{\varepsilon}(t)$, $\bar{\nu}_{\rm ion}(t)$, and $V_r(t)$ are available from the EVDF $f(\mathbf{v},t)$:

$$\bar{\varepsilon}(t) = \frac{1}{n_{\rm e}(t)} \int_{\mathbf{v}} \frac{1}{2} m v^2 f(\mathbf{v},t) d\mathbf{v}, \quad (16)$$

$$\bar{\nu}_{\rm ion}(t) = \frac{1}{n_{\rm e}(t)} \int_{\mathbf{v}} N[q_{\rm ion}(v) - q_{\rm att}(v)] v f(\mathbf{v},t) d\mathbf{v}, \quad (17)$$

$$V_r(t) = \frac{1}{n_{\rm e}(t)} \int_{\mathbf{v}} v_r f(\mathbf{v},t) d\mathbf{v}. \quad (18)$$

$W_x(t)$, $W_y(t)$, and $W_z(t)$ are derived as the time-derivatives of $G_x(t)$, $G_y(t)$, and $G_x(t)$, respectively:

$$W_r(t) = \frac{d}{dt} G_r(t) = \frac{d}{dt} \left[\frac{1}{n_{\rm e}(t)} \int_{\mathbf{v}} m^{\rm L}_{1,r}(\mathbf{v},t) d\mathbf{v} \right]. \quad (19)$$

$\mathbf{W}$ and $\mathbf{V}$ correspond to the 'bulk' and 'flux' drift velocities [23], respectively. $W_r(t)$ can be written with $V_r(t)$ [14] as

$$W_r(t) = V_r(t) + \frac{1}{n_{\rm e}(t)} \int_{\mathbf{v}} N[q_{\rm ion}(v) - q_{\rm att}(v)] v m^{\rm C}_{1,r}(\mathbf{v},t) d\mathbf{v}, \quad (20)$$

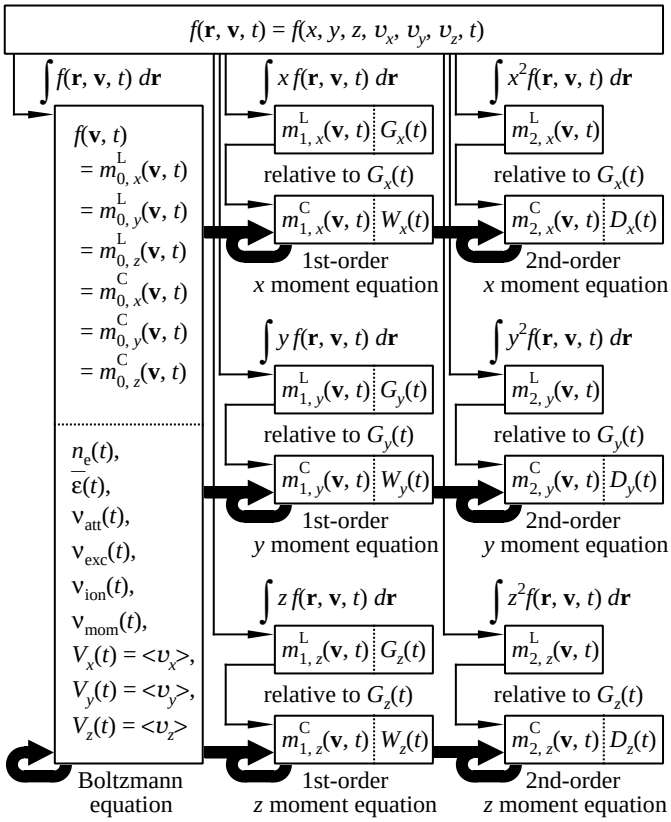

Fig. 2. Derivation paths of moment distribution functions $m^{\rm L}_{n,r}(\mathbf{v},t)$ and $m^{\rm C}_{n,r}(\mathbf{v},t)$ and related electron transport coefficients from $f(\mathbf{r},\mathbf{v},t)$. Relaxation of $m^{\rm C}_{n,r}(\mathbf{v},t)$ proceeds along the thick arrows step by step for $n=0$, 1, and 2. The x, y, and z moment equations are independent of each other.

where N is the gas molecule number density, and $q_{\rm ion}(v)$ and $q_{\rm att}(v)$ are the ionization and attachment collision cross sections, respectively.

As well, $D_x(t)$, $D_y(t)$, and $D_z(t)$ are obtained from the time-derivatives of the second-order moments (or, exactly saying, the second-order cumulants [15]):

$$D_r(t) = \frac{1}{2} \frac{d}{dt} \left[\frac{1}{n_{\rm e}(t)} \int_{\mathbf{v}} m^{\rm C}_{2,r}(\mathbf{v},t) d\mathbf{v} \right]. \quad (21)$$

The relations between the transport coefficients and their source moment distribution functions are shown in Fig. 2 together with their derivation paths from $f(\mathbf{r},\mathbf{v},t)$ and dependence in the numerical scheme. Some primary velocity-space transport coefficients, which can be derived from $f(\mathbf{v},t)$, were calculated in the preceding work [18]. Calculations of the real-space transport coefficients derived from $m^{\rm C}_{n,r}(\mathbf{v},t)$ at $n=1$ and 2 for $r=x$, y, and z are attempted in this paper, and the results were in part reported in Ref. [19].

D. The Boltzmann equation and moment equations

The BE for $f(\mathbf{r},\mathbf{v},t)$ is

$$\frac{\partial}{\partial t} f(\mathbf{r},\mathbf{v},t) = \left[-\mathbf{a}\cdot\frac{\partial}{\partial \mathbf{v}} - \mathbf{v}\cdot\frac{\partial}{\partial \mathbf{r}} + \left(\frac{\partial}{\partial t}\right)_{\rm coll} \right] \times f(\mathbf{r},\mathbf{v},t). \quad (22)$$

The temporal variation of $f(\mathbf{r},\mathbf{v},t)$ is represented by the terms for acceleration, drift, and collision in the right-hand side. By integrating (22) over $\mathbf{r}$, we obtain a BE for the EVDF $f(\mathbf{v},t)$ described only in velocity space:

$$\frac{\partial}{\partial t}f(\mathbf{v},t)=\left[-\mathbf{a}\cdot\frac{\partial}{\partial \mathbf{v}}+\left(\frac{\partial}{\partial t}\right)_{\rm coll}\right]f(\mathbf{v},t). \tag{23}$$

The moment equations for the nth-order moment distribution functions $m^{\rm L}_{n,x}(\mathbf{v},t)$, $m^{\rm L}_{n,y}(\mathbf{v},t)$, and $m^{\rm L}_{n,z}(\mathbf{v},t)$ (denoted as $m^{\rm L}_{n,r}(\mathbf{v},t)$) are also obtained by integrating the BE with weights of x^n, y^n, and z^n (denoted as r^n) over $\mathbf{r}$, respectively [14], [15]:

$$\begin{aligned}\frac{\partial}{\partial t}m^{\rm L}_{n,r}(\mathbf{v},t) &= -\mathbf{a}\cdot\frac{\partial}{\partial \mathbf{v}}m^{\rm L}_{n,r}(\mathbf{v},t)+nv_r m^{\rm L}_{n-1,r}(\mathbf{v},t)\\ &\quad+\left(\frac{\partial}{\partial t}\right)_{\rm coll}m^{\rm L}_{n,r}(\mathbf{v},t).\end{aligned} \tag{24}$$

The second term in the right-hand side of (24) appears as the drift term representing the moment change due to the electron flight in real space. This term is missing when $n=0$.

By substituting the relations between $m^{\rm L}_{n,r}(\mathbf{v},t)$ and $m^{\rm C}_{n,r}(\mathbf{v},t)$ derived from (13)–(15) into (24), we obtain the first- and second-order moment equations in the centroid system:

$$\begin{aligned}\frac{\partial}{\partial t}m^{\rm C}_{1,r}(\mathbf{v},t) &= -\mathbf{a}\cdot\frac{\partial}{\partial \mathbf{v}}m^{\rm C}_{1,r}(\mathbf{v},t)\\ &\quad+(v_r-W_r)m^{\rm C}_{0,r}(\mathbf{v},t)\\ &\quad+\left(\frac{\partial}{\partial t}\right)_{\rm coll}m^{\rm C}_{1,r}(\mathbf{v},t),\end{aligned} \tag{25}$$

$$\begin{aligned}\frac{\partial}{\partial t}m^{\rm C}_{2,r}(\mathbf{v},t) &= -\mathbf{a}\cdot\frac{\partial}{\partial \mathbf{v}}m^{\rm C}_{2,r}(\mathbf{v},t)\\ &\quad+2(v_r-W_r)m^{\rm C}_{1,r}(\mathbf{v},t)\\ &\quad+\left(\frac{\partial}{\partial t}\right)_{\rm coll}m^{\rm C}_{2,r}(\mathbf{v},t).\end{aligned} \tag{26}$$

Equations (23), (25), and (26) represent the spatial development of the electron swarm. The equilibrium values of the electron transport coefficients are calculated from $m^{\rm C}_{n,r}(\mathbf{v},t)$ after their relaxation. One way to obtain $m^{\rm C}_{n,r}(\mathbf{v},t)$ in equilibrium is to follow their temporal relaxation processes as performed for electron swarms in dc $\mathbf{E}$ fields [14], [15], [16], [17]. On the other hand, the equilibrium solutions of $m^{\rm C}_{n,r}(\mathbf{v},t)$ can be obtained faster by a numerically accelerated relaxation scheme [3] under the following assumptions.

(i) $f(\mathbf{v},t)$ grows exponentially with t as $f(\mathbf{v},t)=F(\mathbf{v})n_{\rm e}(t)$ and $n_{\rm e}(t)=n_{\rm e}(0)\exp(\bar{\nu}_{\rm ion}t)$ so that the normalized EVDF $F(\mathbf{v})=f(\mathbf{v},t)/n_{\rm e}(t)$ is time-invariant. Thus,

$$\frac{\partial}{\partial t}f(\mathbf{v},t)=\frac{\partial}{\partial t}[f(\mathbf{v},0)\exp(\bar{\nu}_{\rm ion}t)]=\bar{\nu}_{\rm ion}f(\mathbf{v},t). \tag{27}$$

Here, $t=0$ is such a time that the electron swarm can be regarded to be in equilibrium for $t\geq 0$.

(ii) $m^{\rm C}_{1,r}(\mathbf{v},t)$ also grows exponentially with t as

$$\frac{\partial}{\partial t}m^{\rm C}_{1,r}(\mathbf{v},t)=\frac{\partial}{\partial t}[m^{\rm C}_{1,r}(\mathbf{v},0)\exp(\bar{\nu}_{\rm ion}t)]=\bar{\nu}_{\rm ion}m^{\rm C}_{1,r}(\mathbf{v},t) \tag{28}$$

so that W_r in (20) derived from the normalized first-order moment distribution $m^{\rm C}_{1,r}(\mathbf{v},t)/n_{\rm e}(t)$ is time-invariant.

(iii) $m^{\rm C}_{2,r}(\mathbf{v},t)$ increases as

$$\frac{\partial}{\partial t}m^{\rm C}_{2,r}(\mathbf{v},t)=\bar{\nu}_{\rm ion}m^{\rm C}_{2,r}(\mathbf{v},t)+2D_r m^{\rm C}_{0,r}(\mathbf{v},t) \tag{29}$$

so that D_r in (21) derived from the normalized second-order moment distribution $m^{\rm C}_{2,r}(\mathbf{v},t)/n_{\rm e}(t)$ is time-invariant.

These assumptions are utilized in the numerical relaxation of $m^{\rm C}_{n,r}(\mathbf{v})$ in the PM as presented in section III-D.

III. Propagator method

Practical PM calculation is performed for the sub-ensembles of $m^{\rm C}_{n,r}(\mathbf{v})$. The sub-ensembles are defined in each cell obtained by partitioning of velocity space. After the convergence of the sub-ensembles to their equilibrium solutions, the real-space electron transport coefficients are derived by integrating the sub-ensembles with appropriate weights given as properties associated with the cells.

A. Cells and associated quantities

Velocity space (v,θ,ϕ) represented with polar coordinates is divided into cells with section widths $\Delta\varepsilon=\varepsilon_{\max}/i_{\max}$ for v, $\Delta\theta=\pi/j_{\max}$ for θ, and $\Delta\phi=2\pi/k_{\max}$ for ϕ. Here, a uniform division for electron energy $\varepsilon=\frac{1}{2}mv^2$ results in non-uniform division for v. With $v_i=v_{1\rm eV}\sqrt{i\Delta\varepsilon/\varepsilon_{1\rm eV}}$ ($v_{1\rm eV}$ is the electron speed associated with 1 eV), $\varepsilon_{1\rm eV}=\frac{1}{2}mv^2_{1\rm eV}=1\,$eV, $\theta_j=j\Delta\theta$, and $\phi_k=k\Delta\phi$, the region occupied by the (i,j,k)th cell $C_{i,j,k}$ ($1\leq i\leq i_{\max}$, $1\leq j\leq j_{\max}$, and $1\leq k\leq k_{\max}$) is defined as

$$C_{i,j,k}:\ v_{i-1}\leq v\leq v_i,\ \theta_{j-1}\leq\theta\leq\theta_j,\ \phi_{k-1}\leq\phi\leq\phi_k. \tag{30}$$

A schematic of the cell configuration is shown in Fig. 3 together with the electron acceleration vector $\mathbf{a}$ in velocity space projected to the v_xv_z-plane. The numbers of sections $i_{\max}$, $j_{\max}$, and $k_{\max}$ and the energy range $\varepsilon_{\max}$ for the EVDF calculation are chosen depending on the strengths of $\mathbf{E}$ and $\mathbf{B}$ fields and required resolution. It is convenient to let $k_{\max}$ be a multiple of four so that cell boundaries are aligned at the v_xv_y- and v_yv_z-planes to simplify the treatment of the acceleration propagator explained in section III-C.

The volume $V_{i,j,k}$ of $C_{i,j,k}$ in velocity space is

$$\begin{aligned}V_{i,j,k} &= \int_{v_{i-1}}^{v_i}\int_{\theta_{j-1}}^{\theta_j}\int_{\phi_{k-1}}^{\phi_k}v^2\sin\theta\,dvd\theta d\phi\\ &= \frac{1}{3}(v_i^3-v_{i-1}^3)(\cos\theta_{j-1}-\cos\theta_j)(\phi_k-\phi_{k-1}).\end{aligned} \tag{31}$$

The solid angle $\Omega_{j,k}$ of $C_{i,j,k}$ subtended at the origin O of velocity space is

$$\begin{aligned}\Omega_{j,k} &= \int_{\theta_{j-1}}^{\theta_j}\int_{\phi_{k-1}}^{\phi_k}\sin\theta\,d\theta d\phi\\ &= (\cos\theta_{j-1}-\cos\theta_j)(\phi_k-\phi_{k-1}).\end{aligned} \tag{32}$$

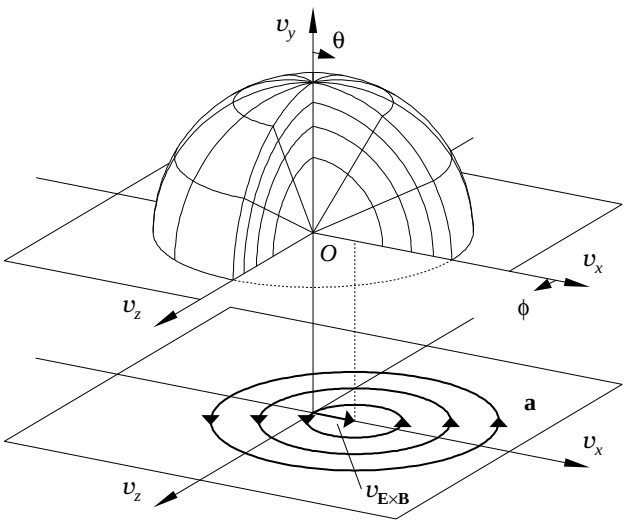

Fig. 3. Cells defined in velocity space and electron acceleration $\mathbf{a}$ projected to the v_xv_z-plane. The cells in the half-space of $v_y \leq 0$ can be omitted under $\mathbf{E} \perp \mathbf{B}$ for the reflective symmetry of the equilibrium solution with respect to the v_xv_z-plane. The cells in the octant of $v_x \geq 0$, $v_y \geq 0$, and $v_z \geq 0$ are not drawn to show inner cells. $\mathbf{a}$ is rotational but off-centered from the v_y-axis. The shift of its rotation center corresponds to the $\mathbf{E} \times \mathbf{B}$ drift velocity $v_{\mathbf{E}\times\mathbf{B}} = E/B$.

As the properties associated with $C_{i,j,k}$, let us define the total amounts of the nth-order r-direction moments within $C_{i,j,k}$ as $\mu^{\mathrm{L}}_{n,r,i,j,k}$ and $\mu^{\mathrm{C}}_{n,r,i,j,k}$:

$$\mu^{\mathrm{L}}_{n,r,i,j,k} = \int_{C_{i,j,k}} m^{\mathrm{L}}_{n,r}(\mathbf{v},t)d\mathbf{v}, \tag{33}$$

$$\mu^{\mathrm{C}}_{n,r,i,j,k} = \int_{C_{i,j,k}} m^{\mathrm{C}}_{n,r}(\mathbf{v},t)d\mathbf{v}. \tag{34}$$

$\mu^{\mathrm{L}}_{0,r,i,j,k} = \mu^{\mathrm{C}}_{0,r,i,j,k}$ is the number of electrons $n_{\mathrm{e},i,j,k}$ in $C_{i,j,k}$. $\mu^{\mathrm{C}}_{n,r,i,j,k}$ is the very quantity to be relaxed in the practical PM calculation. The electron transport coefficients defined in (16)–(18), (20), and (21) are obtained after the relaxation of $\mu^{\mathrm{C}}_{n,r,i,j,k}$ by summing them up.

We can omit the cells in the half-space of $v_y < 0$ in the PM calculation for the reflectional symmetry of the equilibrium solutions of the moment distribution functions with respect to the v_xv_z-plane, when $\mathbf{E} \perp \mathbf{B}$:

$$\mu^{\mathrm{C}}_{n,r,i,j,k} = -\mu^{\mathrm{C}}_{n,r,i,j_{\max}-j+1,k} \quad (\text{for } r = y \text{ at odd } n), \tag{35}$$

$$\mu^{\mathrm{C}}_{n,r,i,j,k} = \mu^{\mathrm{C}}_{n,r,i,j_{\max}-j+1,k} \quad (\text{for the other cases}). \tag{36}$$

$C_{i,j,k}$ has representative values $\varepsilon^{\mathrm{R}}_i$, v^{R}_i, θ^{R}_j, and ϕ^{R}_k:

$$\varepsilon^{\mathrm{R}}_i = \frac{1}{2}(\varepsilon_{i-1}+\varepsilon_i) = \left(i-\frac{1}{2}\right)\Delta\varepsilon, \tag{37}$$

$$v^{\mathrm{R}}_i = v_{1\mathrm{eV}}\sqrt{\varepsilon^{\mathrm{R}}_i/\varepsilon_{1\mathrm{eV}}}, \tag{38}$$

$$\theta^{\mathrm{R}}_j = \frac{1}{2}(\theta_{j-1}+\theta_j) = \left(j-\frac{1}{2}\right)\Delta\theta, \tag{39}$$

$$\phi^{\mathrm{R}}_k = \frac{1}{2}(\phi_{k-1}+\phi_k) = \left(k-\frac{1}{2}\right)\Delta\phi. \tag{40}$$

$(v^{\mathrm{R}}_i, \theta^{\mathrm{R}}_j, \phi^{\mathrm{R}}_k)$ represents the effective center of $C_{i,j,k}$ for the derivation of electron transport coefficients from $\mu^{\mathrm{L}}_{n,r,i,j,k}$ and $\mu^{\mathrm{C}}_{n,r,i,j,k}$.

$C_{i,j,k}$ has six boundaries facing to the $\pm v$, $\pm\theta$, and $\pm\phi$ directions. Let us name them $B^{\pm v}_{i,j,k}$, $B^{\pm\theta}_{i,j,k}$, and $B^{\pm\phi}_{i,j,k}$, respectively:

$$B^{+v}_{i,j,k}:\ v = v_i,\quad \theta_{j-1} \leq \theta \leq \theta_j,\ \phi_{k-1} \leq \phi \leq \phi_k \tag{41}$$

$$B^{-v}_{i,j,k}:\ v = v_{i-1},\ \theta_{j-1} \leq \theta \leq \theta_j,\ \phi_{k-1} \leq \phi \leq \phi_k \tag{42}$$

$$B^{+\theta}_{i,j,k}:\ v_{i-1} \leq v \leq v_i,\ \theta = \theta_j,\quad \phi_{k-1} \leq \phi \leq \phi_k \tag{43}$$

$$B^{-\theta}_{i,j,k}:\ v_{i-1} \leq v \leq v_i,\ \theta = \theta_{j-1},\ \phi_{k-1} \leq \phi \leq \phi_k \tag{44}$$

$$B^{+\phi}_{i,j,k}:\ v_{i-1} \leq v \leq v_i,\ \theta_{j-1} \leq \theta \leq \theta_j,\ \phi = \phi_k \tag{45}$$

$$B^{-\phi}_{i,j,k}:\ v_{i-1} \leq v \leq v_i,\ \theta_{j-1} \leq \theta \leq \theta_j,\ \phi = \phi_{k-1} \tag{46}$$

$B^{\pm v}_{i,j,k}$ are sections on spheres centered at O, and $B^{-v}_{i,j,k} = B^{+v}_{i-1,j,k}$. $B^{\pm\theta}_{i,j,k}$ are sections on cones whose vertices are all at O, and $B^{-\theta}_{i,j,k} = B^{+\theta}_{i,j-1,k}$. $B^{\pm\phi}_{i,j,k}$ are sections on planes including the v_y-axis, and $B^{-\phi}_{i,j,k} = B^{+\phi}_{i,j,k-1}$. They are referred to afterward in the evaluation of the electron outflow from a cell to its neighboring downstream cells for quantification of the acceleration propagator. When $k_{\max}$ is a multiple of four, $B^{+\phi}_{i,j,k}$ at $k = \frac{1}{4}k_{\max}$, $\frac{1}{2}k_{\max}$, $\frac{3}{4}k_{\max}$, and $k_{\max}$ are included in the v_yv_z-plane or the v_xv_y-plane.

B. Collision propagator

The collision propagator $P_{\mathrm{coll}}(C_{i',j',k'} \leftarrow C_{i,j,k})$ represents the electron transfer from $C_{i,j,k}$ to $C_{i',j',k'}$ per unit time due to collision and resulting scattering. More than one cell can be $C_{i',j',k'}$ for one $C_{i,j,k}$. The number of electrons scattered out of $C_{i,j,k}$ per unit time by a process denoted as '$*$' is $Nq_*(v^{\mathrm{R}}_i)n_{i,j,k} = \nu_{i,*}n_{i,j,k}$, where q_* is the electron collision cross section and '$*$' may be 'mom' for momentum transfer (elastic) collision, 'exc' for excitation, 'ion' for ionization, or 'att' for electron attachment in this paper. The scattered electrons are re-distributed to $C_{i',j',k'}$. The energy loss in inelastic collisions is represented as $\varepsilon^{\mathrm{R}}_i - \varepsilon^{\mathrm{R}}_{i'} = (i-i')\Delta\varepsilon$, and the difference $i-i'$ is denoted as l_* for specific collisional processes. The scattering is expressed as the changes of j and k to j' and k', respectively. $P_{\mathrm{coll}}(C_{i',j',k'} \leftarrow C_{i,j,k})$ associated with a collisional process '$*$' is quantified as

$$P_{\mathrm{coll},*}(C_{i',j',k'} \leftarrow C_{i,j,k}) = \nu_{i,*}\delta_{i'}\frac{\Omega_{j',k'}}{4\pi}. \tag{47}$$

Here, $\nu_{i,*} = Nq_*(v^{\mathrm{R}}_i)v^{\mathrm{R}}_i$ is the collision frequency of process '$*$', $\delta_{j'}$ is a division factor for the electron re-distribution for the case i' has a range, and the solid angle factor $\Omega_{j',k'}/(4\pi)$ represents isotropic scattering. The values of these factors in $P_{\mathrm{coll}}(C_{i',j',k'} \leftarrow C_{i,j,k})$ for specific collisional processes are listed in table I.

In the present extension of the PM for moment equations, $P_{\mathrm{coll}}(C_{i',j',k'} \leftarrow C_{i,j,k})$ is common for operator $(\partial/\partial t)_{\mathrm{coll}}$ in all orders n, because the amount of moment transferred by electrons from a cell to another is proportional to the number of scattered electrons.

TABLE I
FACTORS IN COLLISION PROPAGATOR $P_{\mathrm{coll},*}(C_{i',j',k'} \leftarrow C_{i,j,k}) = \nu_{i,*}\delta_{j'}\Omega_{j',k'}/(4\pi)$ [3].

Collisions	ε_*	l_*	$\nu_{i,*}$	i'	$\delta_{i'}$
momentum transfer	0	$l_{\mathrm{mom}} = 0$	$Nq_{\mathrm{mom}}(v_i^{\mathrm{R}})v_i^{\mathrm{R}}$	$i' = i$	1
excitation	$\varepsilon_{\mathrm{exc}}$	$l_{\mathrm{exc}} = \lfloor \varepsilon_{\mathrm{exc}}/\Delta\varepsilon \rfloor$	$Nq_{\mathrm{exc}}(v_i^{\mathrm{R}})v_i^{\mathrm{R}}$	$i' = i - l_{\mathrm{exc}}$	1
ionization	$\varepsilon_{\mathrm{ion}}$	$l_{\mathrm{ion}} = \lfloor \varepsilon_{\mathrm{ion}}/\Delta\varepsilon \rfloor$	$Nq_{\mathrm{ion}}(v_i^{\mathrm{R}})v_i^{\mathrm{R}}$	$i' = i - l_{\mathrm{ion}}$	$2/[2(i - l_{\mathrm{ion}}) - 1]$
				$i' < i - l_{\mathrm{ion}}$	$4/[2(i - l_{\mathrm{ion}}) - 1]$
electron attachment	—	—	$Nq_{\mathrm{att}}(v_i^{\mathrm{R}})v_i^{\mathrm{R}}$	—	0

'$*$' represents a process among momentum transfer, excitation, ionization, and electron attachment.

C. Acceleration propagator

The acceleration propagator $P_{\mathrm{acc}}(C_{i',j',k'} \leftarrow C_{i,j,k})$, i.e., the number of electrons transferred from $C_{i,j,k}$ to $C_{i',j',k'}$ per unit time by the Coulomb and Lorentz forces, has a non-zero value when $C_{i,j,k}$ and $C_{i',j',k'}$ are contacting and $C_{i,j,k}$ locates in the upstream of $C_{i',j',k'}$; otherwise, $P_{\mathrm{acc}}(C_{i',j',k'} \leftarrow C_{i,j,k}) = 0$. $P_{\mathrm{acc}}(C_{i',j',k'} \leftarrow C_{i,j,k})$ is obtained by the areal integral of the electron flux across the boundary between $C_{i,j,k}$ and $C_{i',j',k'}$ as the rate coefficient:

$$P_{\mathrm{acc}}(C_{i',j',k'} \leftarrow C_{i,j,k}) = \frac{1}{V_{i,j,k}} \int_s \max(\mathbf{a}\cdot\mathbf{n}, 0) ds. \quad (48)$$

Note that the electron flux in velocity space is quantified as the product between the electron number density in the dimensions of (speed)$^{-3}$ and flow speed in speed/time. Here, $\mathbf{n}$ is a unit vector outward from $C_{i,j,k}$ and is normal to the boundary between $C_{i,j,k}$ and $C_{i',j',k'}$. The areal element ds has the dimensions of (speed)^2.

Only the positive values of $\mathbf{a}\cdot\mathbf{n}$ are integrated to quantify the electron outflow from $C_{i,j,k}$, because the direction of $\mathbf{a}$ across a cell boundary may change even within the boundary. That is, mutual inflow and outflow between $C_{i,j,k}$ and $C_{i',j',k'}$ may occur. In case the mutual flows occur, they should be calculated separately instead of the net inflow/outflow, because the electron number density, to which the electron flux is proportional, is different for every source cell.

Similarly to the collision propagator, $P_{\mathrm{acc}}(C_{i',j',k'} \leftarrow C_{i,j,k})$ is also common for the moment equations of all orders.

D. Relaxation scheme

Equations (23), (25), and (26) are discretized for $\mu^{\mathrm{C}}_{n,r,i,j,k}$ defined in (34). The solutions of $\mu^{\mathrm{C}}_{n,r,i,j,k}$ that compose $m^{\mathrm{C}}_{n,r}(\mathbf{v}, t)$ in equilibrium are obtained from balance equations between the outflow and inflow of the nth-order moment for each cell.

The terms of acceleration, collision, and drift for $\mu^{\mathrm{C}}_{n,r,i,j,k}$ can be separated as

$$\begin{aligned}
&\frac{\partial}{\partial t}\mu^{\mathrm{C}}_{n,r,i,j,k} \\
&= \left[\left(\frac{\partial}{\partial t}\right)^{\mathrm{in}}_{\mathrm{acc}} - \left(\frac{\partial}{\partial t}\right)^{\mathrm{out}}_{\mathrm{acc}} + \left(\frac{\partial}{\partial t}\right)^{\mathrm{in}}_{\mathrm{coll}} - \left(\frac{\partial}{\partial t}\right)^{\mathrm{out}}_{\mathrm{coll}} \right. \\
&\quad \left. + \left(\frac{\partial}{\partial t}\right)_{\mathrm{drift}}\right] \times \mu^{\mathrm{C}}_{n,r,i,j,k}. \quad (49)
\end{aligned}$$

The outflows $(\partial/\partial t)^{\mathrm{out}}_{\mathrm{acc}}\mu^{\mathrm{C}}_{n,r,i,j,k}$ and $(\partial/\partial t)^{\mathrm{out}}_{\mathrm{coll}}\mu^{\mathrm{C}}_{n,r,i,j,k}$ are proportional to $\mu^{\mathrm{C}}_{n,r,i,j,k}$ as

$$\begin{aligned}
&\left(\frac{\partial}{\partial t}\right)^{\mathrm{out}}_{\mathrm{acc}} \mu^{\mathrm{C}}_{n,r,i,j,k} \\
&= \sum_{B=B^{\pm v}_{i,j,k}, B^{\pm\theta}_{i,j,k}, B^{\pm\phi}_{i,j,k}} \frac{\int_B \max(\mathbf{a}\cdot\mathbf{n}, 0) ds}{V_{i,j,k}} \mu^{\mathrm{C}}_{n,r,i,j,k}, \quad (50)
\end{aligned}$$

$$\begin{aligned}
&\left(\frac{\partial}{\partial t}\right)^{\mathrm{out}}_{\mathrm{coll}} \mu^{\mathrm{C}}_{n,r,i,j,k} \\
&= (\nu_{\mathrm{mom}} + \nu_{\mathrm{exc}} + \nu_{\mathrm{ion}} + \nu_{\mathrm{att}})\mu^{\mathrm{C}}_{n,r,i,j,k} \\
&= \nu_{\mathrm{total}}\mu^{\mathrm{C}}_{n,r,i,j,k}. \quad (51)
\end{aligned}$$

On the other hand, the inflows $(\partial/\partial t)^{\mathrm{in}}_{\mathrm{acc}}\mu^{\mathrm{C}}_{n,r,i,j,k}$ and $(\partial/\partial t)^{\mathrm{in}}_{\mathrm{coll}}\mu^{\mathrm{C}}_{n,r,i,j,k}$ are dependent on $\mu^{\mathrm{C}}_{n,r,i',j',k'}$ of cells other than $C_{i,j,k}$ as

$$\begin{aligned}
&\left(\frac{\partial}{\partial t}\right)^{\mathrm{in}}_{\mathrm{acc}} \mu^{\mathrm{C}}_{n,r,i,j,k} \\
&= \frac{\int_{B^{-v}_{i+1,j,k}} \max(\mathbf{a}\cdot\mathbf{n}, 0) ds}{V_{i+1,j,k}} \mu^{\mathrm{C}}_{n,r,i+1,j,k} \\
&\quad + \frac{\int_{B^{+v}_{i-1,j,k}} \max(\mathbf{a}\cdot\mathbf{n}, 0) ds}{V_{i-1,j,k}} \mu^{\mathrm{C}}_{n,r,i-1,j,k} \\
&\quad + \frac{\int_{B^{-\theta}_{i,j+1,k}} \max(\mathbf{a}\cdot\mathbf{n}, 0) ds}{V_{i,j+1,k}} \mu^{\mathrm{C}}_{n,r,i,j+1,k} \\
&\quad + \frac{\int_{B^{+\theta}_{i,j-1,k}} \max(\mathbf{a}\cdot\mathbf{n}, 0) ds}{V_{i,j-1,k}} \mu^{\mathrm{C}}_{n,r,i,j-1,k} \\
&\quad + \frac{\int_{B^{-\phi}_{i,j,k+1}} \max(\mathbf{a}\cdot\mathbf{n}, 0) ds}{V_{i,j,k+1}} \mu^{\mathrm{C}}_{n,r,i,j,k+1} \\
&\quad + \frac{\int_{B^{+\phi}_{i,j,k-1}} \max(\mathbf{a}\cdot\mathbf{n}, 0) ds}{V_{i,j,k-1}} \mu^{\mathrm{C}}_{n,r,i,j,k-1}, \quad (52)
\end{aligned}$$

$$\begin{aligned}
&\left(\frac{\partial}{\partial t}\right)^{\mathrm{in}}_{\mathrm{coll}} \mu^{\mathrm{C}}_{n,r,i,j,k}, \\
&= \sum_{i',j',k'} P_{\mathrm{coll}}(C_{i,j,k} \leftarrow C_{i',j',k'}) \mu^{\mathrm{C}}_{n,r,i',j',k'}. \quad (53)
\end{aligned}$$

Here, the direction of $\mathbf{n}$ is outward from the source cells. Note that some terms in the right-hand side of (52) may be ignored when one of the indices i and j is out of their definition range (e.g., no $\mu^{\mathrm{C}}_{n,r,i-1,j,k}$ when $i = 1$, and no $\mu^{\mathrm{C}}_{n,r,i,j-1,k}$ when $j = 1$), and the quantities corresponding to $k = 0$ and

$k = k_{\max}+1$ are interpreted as those of $k = k_{\max}$ and $k = 1$, respectively, because k for ϕ is cyclic.

Furthermore, the drift term $(\partial/\partial t)_{\rm drift}\mu^{\rm C}_{n,r,i,j,k}$, is proportional to a lower-order moment $\mu^{\rm C}_{n-1,r,i,j,k}$ as

$$\left(\frac{\partial}{\partial t}\right)_{\rm drift}\mu^{\rm C}_{n,r,i,j,k} = n(v^{\rm R}_{r,i,j,k} - W_r)\mu^{\rm C}_{n-1,r,i,j,k}. \quad (54)$$

This term appears for $n \geq 1$ and is newly introduced in this work to the PM calculation under the $\mathbf{E}\times\mathbf{B}$ fields. Here, $v^{\rm R}_{r,i,j,k}$ is one of the representative values of $v^{\rm R}_{x,i,j,k}$, $v^{\rm R}_{y,i,j,k}$, and $v^{\rm R}_{z,i,j,k}$ defined for $C_{i,j,k}$ as

$$v^{\rm R}_{x,i,j,k} = v^{\rm R}_i \sin\theta^{\rm R}_j \cos\phi^{\rm R}_k, \quad (55)$$
$$v^{\rm R}_{y,i,j,k} = v^{\rm R}_i \cos\theta^{\rm R}_j, \quad (56)$$
$$v^{\rm R}_{z,i,j,k} = v^{\rm R}_i \sin\theta^{\rm R}_j \sin\phi^{\rm R}_k. \quad (57)$$

Under assumptions (i), (ii), and (iii) in section II-D, which are described as (27)–(29), $\mu^{\rm C}_{n,r,i,j,k}$ in (49) satisfies the following equation on the balance between the outflow and inflow in equilibrium [3]:

$$\mu^{\rm C}_{n,r,i,j,k} = \frac{\left[(\partial/\partial t)^{\rm in}_{\rm acc} + (\partial/\partial t)^{\rm in}_{\rm coll} + (\partial/\partial t)_{\rm drift}\right]\mu^{\rm C}_{n,r,i,j,k}}{\partial/\partial t + (\partial/\partial t)^{\rm out}_{\rm acc} + (\partial/\partial t)^{\rm out}_{\rm coll}}. \quad (58)$$

The terms in the numerator of the right-hand side are practically represented by moments other than $\mu^{\rm C}_{n,r,i,j,k}$ as shown in (52)–(54). Explicit forms of (58) at specific orders $n = 0$, 1, and 2 are

$$\mu^{\rm C}_{0,r,i,j,k} = \frac{1}{R}\sum_{i',j',k'} P_{\rm acc}(C_{i,j,k} \leftarrow C_{i',j',k'})\mu^{\rm C}_{0,r,i',j',k'} + \frac{1}{R}\sum_{i',j',k'} P_{\rm coll}(C_{i,j,k} \leftarrow C_{i',j',k'})\mu^{\rm C}_{0,r,i',j',k'}, \quad (59)$$

$$\mu^{\rm C}_{1,r,i,j,k} = \frac{1}{R}\sum_{i',j',k'} P_{\rm acc}(C_{i,j,k} \leftarrow C_{i',j',k'})\mu^{\rm C}_{1,r,i',j',k'} + \frac{1}{R}\sum_{i',j',k'} P_{\rm coll}(C_{i,j,k} \leftarrow C_{i',j',k'})\mu^{\rm C}_{1,r,i',j',k'} + \frac{1}{R}(v_{r,i,j,k} - W_r)\mu^{\rm C}_{0,r,i,j,k}, \quad (60)$$

$$\mu^{\rm C}_{2,r,i,j,k} = \frac{1}{R}\sum_{i',j',k'} P_{\rm acc}(C_{i,j,k} \leftarrow C_{i',j',k'})\mu^{\rm C}_{2,r,i',j',k'} + \frac{1}{R}\sum_{i',j',k'} P_{\rm coll}(C_{i,j,k} \leftarrow C_{i',j',k'})\mu^{\rm C}_{2,r,i',j',k'} + \frac{1}{R}2(v_{r,i,j,k} - W_r)\mu^{\rm C}_{1,r,i,j,k} - \frac{1}{R}2D_r\mu^{\rm C}_{0,r,i,j,k}, \quad (61)$$

where

$$R = \bar{\nu}_{\rm ion}(v^{\rm R}_i) + \sum_{i',j',k'} P_{\rm acc}(C_{i',j',k'} \leftarrow C_{i,j,k}) + \nu_{\rm total}(v^{\rm R}_i). \quad (62)$$

Initial distributions of the nth-order moments are given to $\mu^{\rm C}_{n,r,i,j,k}$, and they are relaxed in the manner of the Gauss–Seidel method. The relaxation is terminated when the relative change of the electron transport coefficient specific to the order n within a relaxation cycle is sufficiently small (e.g., $< 10^{-7}$).

The sequence of the relaxation of $\mu^{\rm C}_{n,r,i,j,k}$ for the order n and the direction r was as follows.

1) Relaxation of the EVDF: A typical initial distribution is a Maxwellian distribution. $f(\mathbf{v})$ is relaxed by iteratively operating (59) to obtain the normalized EVDF $F(\mathbf{v}) = f(\mathbf{v})/\int f(\mathbf{v})d\mathbf{v}$ in equilibrium. This is the solution of the BE by the PM for velocity-space electron transport coefficients [18]. The convergence of $F(\mathbf{v})$ can be judged with those of $\bar{\varepsilon}$, $\bar{\nu}_{\rm ion}$, and V_r derived from $f(\mathbf{v})$.
2) Relaxation of the first-order moment distribution function: A possible initial distribution is $m^{\rm C}_{1,r}(\mathbf{v}) = 0$, which corresponds to electrons supplied from a point source. $m^{\rm C}_{1,r}(\mathbf{v})$ is relaxed by iteratively operating (60) to obtain the normalized first-order moment distribution function $M_{1,r}(\mathbf{v}) = m^{\rm C}_{1,r}(\mathbf{v})/\int m^{\rm C}_{1,r}(\mathbf{v})d\mathbf{v}$ under the already obtained $F(\mathbf{v})$. Because W_r to be derived from $M_{1,r}(\mathbf{v})$ is included in (60), W_r is also renewed every relaxation cycle. The convergence of $M_{1,r}(\mathbf{v})$ can be judged with that of W_r. An exception is that the convergence of $M_{1,y}(\mathbf{v})$ is judged with that of W'_y because $W_y = W_{\mathbf{B}}$ is always zero under $\mathbf{E}\perp\mathbf{B}$, where W'_y is the y-direction centroid drift velocity of the electrons with $v_y \geq 0$ and W'_y is obtained by limiting the region of the integrals in (10), (18), and (20) to be $v_y \geq 0$.
3) Relaxation of the second-order moment distribution function: A possible initial distribution is $m^{\rm C}_{2,r}(\mathbf{v}) = 0$ similarly to the first-order moment distribution. $m^{\rm C}_{2,r}(\mathbf{v})$ is relaxed by iteratively operating (61) under the already obtained $F(\mathbf{v})$ and $M_{1,r}(\mathbf{v})$ until D_r derived from $m^{\rm C}_{2,r}(\mathbf{v})$ reaches a constant value. Because D_r has usually a positive value, the normalized second-order moment distribution function $M_{2,r}(\mathbf{v}) = m^{\rm C}_{2,r}(\mathbf{v})/\int_{\mathbf{v}} m^{\rm C}_{2,r}(\mathbf{v})d\mathbf{v}$ increases with time even in equilibrium. Thus, $M_{2,r}(\mathbf{v})$ does not converge to a specific value.

The dependence of the moment distribution functions at different orders in the hierarchy is shown in Fig. 2. The series of moments in one of the x, y, and z directions are independent of those in the different directions.

The renewal of the $\mu^{\rm C}_{n,r,i,j,k}$ values in the relaxation at each combination of n and r is applied basically from the upstream of the electron acceleration (i.e., electron flow in velocity space) towards the downstream along the direction of $\mathbf{a}$. The indices i, j, and k change by increment or decrement in a triple nesting loop structure in the PM program. The directions in which i and j run are fixed corresponding to the octant that $C_{i,j,k}$ belongs to. However, the change of k is partly exceptional for two reasons; the series of cells are cyclic in the ϕ direction, and the upstream and downstream are partly reverse for ϕ. The reverse region is the inside of a cylinder: $[v_x - E/(2B)]^2 + v_z^2 < [E/(2B)]^2$. The electron flow through $B^{+\phi}_{i,j,k}$ due to $\mathbf{a}$ is from the $+\phi$ side to the $-\phi$ side when $B^{+\phi}_{i,j,k}$ is outside of the cylinder, and is from the $-\phi$ side to the $+\phi$ side when $B^{+\phi}_{i,j,k}$ is in the cylinder.

The renewal sequence of $\mu^{\mathrm{C}}_{n,r,i,j,k}$ for i, j, and k was arranged as follows.

1) Renewal sequence in the v direction (inner loop): At given j and k values, the renewal is operated from $i = i_{\max}$ ($v = v_{\max}$) to $i = 1$ ($v = 0$) by decrement of i in the region of $v_z \leq 0$, and from $i = 1$ to $i = i_{\max}$ by increment of i in the region of $v_z \geq 0$.
2) Renewal sequence in the θ direction (middle loop): At a given k value, the renewal is operated from $j = \frac{1}{2}j_{\max}$ ($\theta = \frac{1}{2}\pi$) to $j = 1$ ($\theta = 0$) by decrement of j in the region of $v_z \leq 0$, and from $j = 1$ to $j = \frac{1}{2}j_{\max}$ by increment of j in the region of $v_z \geq 0$.
3) Renewal sequence in the ϕ direction (outer loop): The following forward and reverse cycles alternate every other relaxation cycles. In the forward cycle, the renewal is operated from $k = k_{\max}$ ($\phi = 2\pi$) to $k = 1$ ($\phi = 0$) by decrement of k. In the reverse cycle, the renewal for the cells in the region of $v_x < 0$ is unchanged; from $k = \frac{3}{4}k_{\max}$ ($\phi = \frac{3}{2}\pi$) to $k = \frac{1}{4}k_{\max} + 1$ ($\phi = \frac{1}{2}\pi$) by decrement of k. On the other hand, that for the cells in the region of $v_x > 0$ is operated from $k = \frac{3}{4}k_{\max} + 1$ to $k = k_{\max}$ by increment of k and from $k = 1$ to $k = \frac{1}{4}k_{\max}$ by increment of k.

This sequence was adopted in the EVDF relaxation [18], and is applied here also to the relaxations of $m^{\mathrm{C}}_{1,r}(\mathbf{v})$ and $m^{\mathrm{C}}_{2,r}(\mathbf{v})$ in the same manner.

IV. Benchmark

A. Conditions

SF_6 was chosen for benchmark of the present PM calculation. The set of collision cross sections taken from Refs. [24], [25] includes collisional processes of momentum transfer, excitation, ionization, and electron attachment. The latter two processes make the electron swarm non-conservative. They induce the difference between electron transport coefficients defined in velocity space and real space, e.g., $\mathbf{W} \neq \mathbf{V}$ as understood from (20).

The electron transport coefficients were calculated at $E/N = 100$, 200, 500, and 1000 Td (1 Td (townsend) = 10^{-21} Vm^2) and at $B/N = 100$, 200, 500, and 1000 Hx (1 Hx (huxley) = 10^{-27} Tm^3) by the PM. These E/N and B/N values are the same as examined in Refs. [18], [19].

The size of the three-dimensional arrays used in the PM, $i_{\max} \times \frac{1}{2}j_{\max} \times k_{\max}$, was chosen to be $10000 \times 45 \times 720$. The cells were prepared only for the region of $v_y \geq 0$, because the EVDF and moment distribution functions are in reflectional symmetry with respect to the v_xv_z-plane when $\mathbf{E} \perp \mathbf{B}$. This saves the memory capacity for the PM calculation. Although $W_y = W_{\mathbf{B}}$ derived from $m^{\mathrm{C}}_{1,y}(\mathbf{v})$ is always zero for the symmetry, the calculation of $m^{\mathrm{C}}_{1,y}(\mathbf{v})$ is necessary because $m^{\mathrm{C}}_{1,y}(\mathbf{v})$ itself has non-zero values and $m^{\mathrm{C}}_{1,y}(\mathbf{v})$ is referred to in the second-order moment equation for $m^{\mathrm{C}}_{2,y}(\mathbf{v})$.

The benchmark simulations of the PM were carried out with a workstation having the following properties: CPU, Intel Xeon E5-1650 v4 (3.6 GHz); main memory, 128 GB; operating system, Linux CentOS 7.3; programming language, C++.

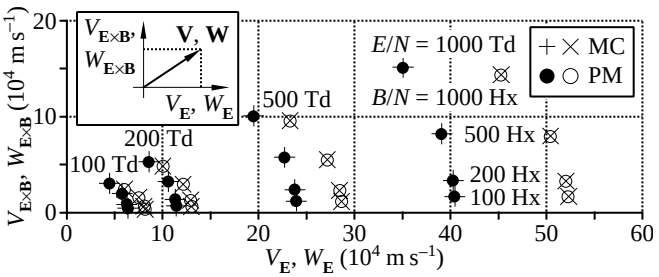

Fig. 4. Drift velocity vectors. • and +, average velocity ($V_{\mathbf{E}}, V_{\mathbf{E}\times\mathbf{B}}$); and ○ and ×, centroid drift velocity ($W_{\mathbf{E}}, W_{\mathbf{E}\times\mathbf{B}}$). Monte Carlo simulation (MC, + and ×) and propagator method (PM, • and ○).

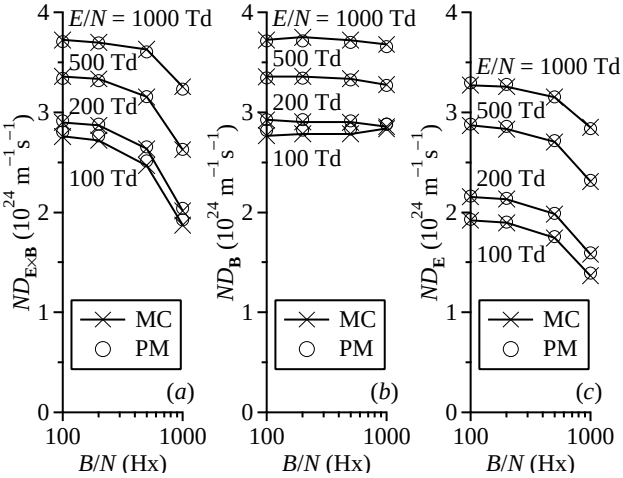

Fig. 5. Diffusion coefficients defined in the directions of (a) $\mathbf{E} \times \mathbf{B}$, ($b$) $\mathbf{B}$ and (c) $\mathbf{E}$. Monte Carlo simulation (MC, ×) and propagator method (PM, ○).

The calculation results were compared with those obtained by MC simulations performed with this workstation and in part with another used for a previous work [18], which had a CPU of Intel Xeon E5-2667 (2.9 GHz) and Linux CentOS 6.4. In the MC simulations, the time step Δt was set at 0.1 ps at $N = 10^{22}$ m^{-3}. The electron transport coefficients reached their equilibrium values by $t =$ 100–200 ns. The number of electrons sampled at the end of the tracking period was more than 10^7. The electron swarm development was attachment-dominated at $E/N = 100$ and 200 Td. These cases were severe for the MC simulation because the electron population decreases during the relaxation period. However, special treatment against the population decrease [26], [27] was not adopted here.

B. Results

The drift velocities $W_{\mathbf{E}\times\mathbf{B}}$ and $W_{\mathbf{E}}$ and the diffusion coefficients $ND_{\mathbf{E}\times\mathbf{B}}$, $ND_{\mathbf{B}}$, and $ND_{\mathbf{E}}$, which have become available with the PM by the present extension, are shown in Figs. 4 and 5. Their values are shown in Table II together with $\bar{\varepsilon}$, $\bar{\nu}_{\mathrm{ion}}/N$, $V_{\mathbf{E}\times\mathbf{B}}$, and $V_{\mathbf{E}}$.

The MC results are the averages during the last 10 ns of each tracking period. Their statistical fluctuations represented as $\sigma_X/\langle X \rangle$ for a quantity X, where σ_X is the standard deviation

TABLE II
THE ELECTRON TRANSPORT COEFFICIENTS IN SF_6.

E/N (Td)	B/N (Hx)	Method	$\bar{\varepsilon}$ (eV)	$\bar{\nu}_{\rm ion}/N$ (10^{-16} m^3 s^{-1})	$V_{\mathbf{E}\times\mathbf{B}}$ (10^4 m s^{-1})	$V_{\mathbf{E}}$	$W_{\mathbf{E}\times\mathbf{B}}$ (10^4 m s^{-1})	$W_{\mathbf{E}}$	$ND_{\mathbf{E}\times\mathbf{B}}$ (10^{24} m^{-1} s^{-1})	$ND_{\mathbf{B}}$	$ND_{\mathbf{E}}$
100	100	MC	5.412	−8.7	0.442	6.392	0.329	8.168	2.76	2.77	1.92
		PM	5.423	−8.9	0.434	6.371	0.339	8.189	2.80	2.82	1.93
	200	MC	5.399	−8.7	0.852	6.289	0.658	8.059	2.72	2.79	1.90
		PM	5.410	−9.0	0.857	6.288	0.669	8.100	2.76	2.82	1.90
	500	MC	5.315	−9.1	1.983	5.783	1.573	7.519	2.47	2.78	1.75
		PM	5.329	−9.4	1.964	5.762	1.530	7.534	2.51	2.83	1.76
	1000	MC	5.112	−10.1	3.046	4.447	2.445	6.023	1.87	2.84	1.36
		PM	5.140	−10.4	3.013	4.442	2.406	6.016	1.92	2.88	1.39
200	100	MC	6.598	−6.4	0.682	11.432	0.628	13.002	2.90	2.93	2.15
		PM	6.603	−6.5	0.692	11.427	0.637	13.036	2.92	2.93	2.16
	200	MC	6.582	−6.4	1.380	11.330	1.263	12.906	2.87	2.91	2.13
		PM	6.586	−6.6	1.371	11.313	1.261	12.919	2.88	2.93	2.14
	500	MC	6.472	−6.7	3.230	10.596	2.954	12.138	2.64	2.90	1.98
		PM	6.476	−6.9	3.217	10.574	2.942	12.159	2.65	2.91	1.99
	1000	MC	6.139	−7.6	5.281	8.559	4.853	10.039	2.02	2.86	1.58
		PM	6.149	−7.8	5.264	8.551	4.825	10.058	2.04	2.88	1.59
500	100	MC	9.320	10.1	1.205	23.927	1.144	28.658	3.36	3.36	2.87
		PM	9.322	10.1	1.198	23.905	1.147	28.650	3.34	3.35	2.88
	200	MC	9.304	9.9	2.382	23.770	2.295	28.450	3.33	3.36	2.83
		PM	9.305	9.9	2.385	23.749	2.282	28.457	3.32	3.34	2.86
	500	MC	9.182	8.9	5.762	22.713	5.489	27.170	3.16	3.34	2.71
		PM	9.183	8.8	5.740	22.685	5.472	27.162	3.16	3.33	2.72
	1000	MC	8.776	5.6	10.077	19.481	9.557	23.289	2.63	3.28	2.31
		PM	8.778	5.6	10.030	19.457	9.522	23.288	2.63	3.27	2.32
1000	100	MC	12.596	74.0	1.675	40.450	1.655	52.285	3.73	3.73	3.27
		PM	12.594	74.0	1.675	40.401	1.634	52.238	3.71	3.72	3.30
	200	MC	12.580	73.6	3.346	40.274	3.272	52.006	3.70	3.75	3.26
		PM	12.579	73.6	3.340	40.227	3.254	52.004	3.70	3.71	3.28
	500	MC	12.469	70.9	8.208	39.077	7.963	50.425	3.63	3.72	3.15
		PM	12.468	71.0	8.176	39.027	7.904	50.400	3.61	3.70	3.15
	1000	MC	12.061	62.1	15.155	35.061	14.347	45.257	3.26	3.68	2.85
		PM	12.062	62.1	15.090	35.036	14.331	45.237	3.23	3.66	2.84

MC: Monte Carlo simulation, and PM: Propagator method.

of X and $\langle X\rangle$ represents the ensemble average of X over the electron swarm, were 1.1–24.4% for $V_{\mathbf{E}\times\mathbf{B}}$, 0.4–0.9% for $V_{\mathbf{E}}$, 0.3–5.5% for $W_{\mathbf{E}\times\mathbf{B}}$, 0.1–0.5% for $W_{\mathbf{E}}$, 1.2–4.7% for $ND_{\mathbf{E}\times\mathbf{B}}$, 1.2–5.3% for $ND_{\mathbf{B}}$, and 1.4–5.3% for $ND_{\mathbf{E}}$. There is a tendency that the fluctuation is larger for the coefficients defined in the $\mathbf{E}\times\mathbf{B}$ direction than for those defined in the $\mathbf{E}$ direction. These uncertainties should be taken into account when the PM and MC results are compared.

Most of the $W_{\mathbf{E}\times\mathbf{B}}$ and $W_{\mathbf{E}}$ values agreed well between the PM and MC results with discrepancies less than 1%. The discrepancy was larger as 1.6–3.3% for $W_{\mathbf{E}\times\mathbf{B}}$ at low E/N of 100 Td. This was perhaps because their absolute values were small. Nonetheless, the PM appropriately calculated the difference between $(W_{\mathbf{E}}, W_{\mathbf{E}\times\mathbf{B}})$ and $(V_{\mathbf{E}}, V_{\mathbf{E}\times\mathbf{B}})$.

$ND_{\mathbf{E}\times\mathbf{B}}$, $ND_{\mathbf{B}}$, and $ND_{\mathbf{E}}$ agreed between the PM and MC with discrepancies up to 2.7%, 2.1%, and 1.9%, respectively. The tendency that discrepancies become larger for $ND_{\mathbf{E}\times\mathbf{B}}$ is common with those on $W_{\mathbf{E}\times\mathbf{B}}$ and its statistical fluctuation. It is suggested that there is some difficulty in the calculations of the moments defined in the direction of $\mathbf{E}\times\mathbf{B}$, toward which the Hall deflection occurs. It is also considered that numerical errors accumulate in the sequence of the relaxation scheme for the moment equations step by step from $n=0$ to $n=2$. However, qualitative dependence of the diffusion coefficients on the E/N and B/N values seen in the MC results was successfully reproduced by the PM as well.

The CPU time spent for the PM calculation in each condition was 6.1–82.9 h. That for the MC simulation was estimated to be 14.3–173.5 h from the ratio of the CPU clock frequencies of the two workstations used. The tendency that the relaxation was slower under lower $\mathbf{E}$ and stronger $\mathbf{B}$ was common for all n values, for all x, y, and z directions, and for both of the PM and MC simulations. The numerical relaxation of $m^{\rm C}_{n,r}(\mathbf{v})$ in the PM was successfully accelerated by alternating the renewal direction of ϕ, i.e., by switching the increment and decrement of index k of $\mu^{\rm C}_{n,r,i,j,k}$, not only at $n=0$ as done in Ref. [18] but also at $n=1$ and 2. The total iteration cycles required for the convergence of the PM solutions were less than $1/10$ of those required in the one-way renewal in the most efficient cases where the diameter of the reverse region, E/B, is relatively large.

V. DISCUSSION

A. Memory saving

The relaxation of $m^{\rm C}_{n,r}(\mathbf{v})$ to obtain the electron transport coefficients in Table II can be performed independently for the x, y, and z directions, where the target diffusion coefficients are defined along the x-, y-, and z-axes (see Fig. 2). A possible relaxation sequence is, for example, in the following order: $F(\mathbf{v})$ $(= m^{\rm C}_{0,x}(\mathbf{v}) = m^{\rm C}_{0,y}(\mathbf{v}) = m^{\rm C}_{0,z}(\mathbf{v}))$, $m^{\rm C}_{1,x}(\mathbf{v})$, $m^{\rm C}_{2,x}(\mathbf{v})$, $m^{\rm C}_{1,y}(\mathbf{v})$, $m^{\rm C}_{2,y}(\mathbf{v})$, $m^{\rm C}_{1,z}(\mathbf{v})$, and $m^{\rm C}_{2,z}(\mathbf{v})$. After the derivations of W_x from $m^{\rm C}_{1,x}(\mathbf{v})$ and D_x from $m^{\rm C}_{2,x}(\mathbf{v})$, the values of $m^{\rm C}_{1,x}(\mathbf{v})$ and $m^{\rm C}_{2,x}(\mathbf{v})$ are no longer necessary for

the succeeding derivations of W_y, D_y, W_z, and D_z. The arrays used for the calculations of $m^{\rm C}_{1,x}(\mathbf{v})$ and $m^{\rm C}_{2,x}(\mathbf{v})$ can be freed and the values of $m^{\rm C}_{1,y}(\mathbf{v})$ and $m^{\rm C}_{2,y}(\mathbf{v})$ can be overwritten on the arrays. This applies again also to the calculations of $m^{\rm C}_{1,z}(\mathbf{v})$ and $m^{\rm C}_{2,z}(\mathbf{v})$ after the derivations of W_y from $m^{\rm C}_{1,y}(\mathbf{v})$ and D_y from $m^{\rm C}_{2,y}(\mathbf{v})$. There is no need to prepare different arrays for all of the x, y, and z moments. The entire calculation can be carried out with at least three arrays for $m^{\rm C}_{n,r}(\mathbf{v})$, except for the arrays for the associated quantities such as the acceleration propagator. The acceleration propagator requires at least four arrays to quantify the electron outflow through three or four of the six boundaries of each cell.

B. Electron transport coefficients in the Hall drift direction

In the presence of the Hall deflection under the $\mathbf{E}\times\mathbf{B}$ fields, some electron transport coefficients may be defined neither along the x-axis, the y-axis, nor the z-axis but in the direction of the Hall drift, which tilts from the $-\mathbf{E}$ direction to the $\mathbf{E}\times\mathbf{B}$ direction.

The drift velocity in the Hall drift direction, $W_{\rm H}$, is available from $W_{\mathbf{E}}$ and $W_{\mathbf{E}\times\mathbf{B}}$ as $W_{\rm H}=(W^2_{\mathbf{E}}+W^2_{\mathbf{E}\times\mathbf{B}})^{1/2}$. The Hall deflection angle ψ is given as $\psi=\tan^{-1}(W_x/W_z)$. $W_{\rm H}$ can be derived without introducing new terms into the moment equations. On the other hand, the derivation of the diffusion coefficient $D_{\rm H}$ in the Hall drift direction needs a new moment distribution term [28].

$D_{\rm H}$ is defined as

$$\begin{aligned}
&D_{\rm H}(t)\\
&= \frac{1}{2}\frac{d}{dt}\left\{\frac{1}{n_{\rm e}(t)}\int_{\mathbf{v}}\int_{\mathbf{r}}\left[(\mathbf{r}-\mathbf{G}(t))\cdot\mathbf{e}\right]^2 f(\mathbf{r},\mathbf{v},t)d\mathbf{r}d\mathbf{v}\right\}\\
&= \frac{1}{2}\frac{d}{dt}\left\{\frac{1}{n_{\rm e}(t)}\int_{\mathbf{v}}\int_{\mathbf{r}}\left[\sin\psi(x-G_x(t))\right.\right.\\
&\qquad\left.\left.+\cos\psi(z-G_z(t))\right]^2 f(\mathbf{r},\mathbf{v},t)d\mathbf{r}d\mathbf{v}\right\}\\
&= \frac{1}{2}\sin^2\psi\frac{d}{dt}\left[\frac{1}{n_{\rm e}(t)}\int_{\mathbf{v}} m^{\rm C}_{2,x}(\mathbf{v},t)d\mathbf{v}\right]\\
&\quad+\frac{1}{2}\cos^2\psi\frac{d}{dt}\left[\frac{1}{n_{\rm e}(t)}\int_{\mathbf{v}} m^{\rm C}_{2,z}(\mathbf{v},t)d\mathbf{v}\right]\\
&\quad+\sin\psi\cos\psi\frac{d}{dt}\left[\frac{1}{n_{\rm e}(t)}\int_{\mathbf{v}} m^{\rm C}_{2,xz}(\mathbf{v},t)d\mathbf{v}\right]\\
&= \sin^2\psi D_{\mathbf{E}\times\mathbf{B}}(t)+\cos^2\psi D_{\mathbf{E}}(t)\\
&\quad+\sin\psi\cos\psi\frac{d}{dt}\left[\frac{1}{n_{\rm e}(t)}\int_{\mathbf{v}} m^{\rm C}_{2,xz}(\mathbf{v},t)d\mathbf{v}\right], \qquad (63)
\end{aligned}$$

where $\mathbf{e}=\mathbf{W}/|\mathbf{W}|$ is a unit vector in the direction of $\mathbf{W}$, and $m^{\rm C}_{2,xz}(\mathbf{v},t)$ is the second-order moment weighted by x and z:

$$\begin{aligned}
m^{\rm L}_{2,xz}(\mathbf{v},t) &= \int_{\mathbf{r}} xz f(\mathbf{r},\mathbf{v},t)d\mathbf{r}, \qquad (64)\\
m^{\rm C}_{2,xz}(\mathbf{v},t) &= \int_{\mathbf{r}}[x-G_x(t)][z-G_z(t)]f(\mathbf{r},\mathbf{v},t)d\mathbf{r}\\
&= m^{\rm L}_{2,xz}(\mathbf{v},t)\\
&\quad- G_z(t)m^{\rm L}_{1,x}(\mathbf{v},t)\\
&\quad- G_x(t)m^{\rm L}_{1,z}(\mathbf{v},t)\\
&\quad+ G_x(t)G_z(t)f(\mathbf{v},t). \qquad (65)
\end{aligned}$$

The moment equation for $m^{\rm L}_{2,xz}(\mathbf{v},t)$ is obtained by integrating (22) with a weight of xz as

$$\begin{aligned}
\frac{\partial}{\partial t}m^{\rm L}_{2,xz}(\mathbf{v},t) &= -\mathbf{a}\cdot\frac{\partial}{\partial\mathbf{v}}m^{\rm L}_{2,xz}(\mathbf{v},t)\\
&\quad+ v_z m^{\rm L}_{1,x}(\mathbf{v},t)\\
&\quad+ v_x m^{\rm L}_{1,z}(\mathbf{v},t)\\
&\quad+\left(\frac{\partial}{\partial t}\right)_{\rm coll} m^{\rm L}_{2,xz}(\mathbf{v},t). \qquad (66)
\end{aligned}$$

In the centroid system, this moment equation becomes

$$\begin{aligned}
\frac{\partial}{\partial t}m^{\rm C}_{2,xz}(\mathbf{v},t) &= -\mathbf{a}\cdot\frac{\partial}{\partial\mathbf{v}}m^{\rm C}_{2,xz}(\mathbf{v},t)\\
&\quad+ (v_z-W_z)m^{\rm C}_{1,x}(\mathbf{v},t)\\
&\quad+ (v_x-W_x)m^{\rm C}_{1,z}(\mathbf{v},t)\\
&\quad+\left(\frac{\partial}{\partial t}\right)_{\rm coll} m^{\rm C}_{2,xz}(\mathbf{v},t). \qquad (67)
\end{aligned}$$

$m^{\rm C}_{2,xz}(\mathbf{v})$ in equilibrium is to be obtained by relaxation in the PM using discretized $\mu^{\rm C}_{2,xz,i,j,k}$ in the same manner as done for $\mu^{\rm C}_{2,r,i,j,k}$. Because $D_{\rm H}$ is obtained from $m^{\rm C}_{2,x}(\mathbf{v},t)$, $m^{\rm C}_{2,z}(\mathbf{v},t)$, and $m^{\rm C}_{2,xz}(\mathbf{v},t)$ as shown in (63), and the PM calculation for $m^{\rm C}_{2,xz}(\mathbf{v},t)$ refers to the converged $m^{\rm C}_{1,x}(\mathbf{v})$ and $m^{\rm C}_{1,z}(\mathbf{v})$ as in (67), we need a sufficient memory capacity for the arrays to store $\mu^{\rm C}_{1,x,i,j,k}$, $\mu^{\rm C}_{1,z,i,j,k}$, $\mu^{\rm C}_{2,x,i,j,k}$, $\mu^{\rm C}_{2,z,i,j,k}$, and $\mu^{\rm C}_{2,xz,i,j,k}$ simultaneously.

C. Further extension of the PM

One of the further extensions of the PM calculation technique would be for calculation of the electron transport coefficients under $\mathbf{E}$ and $\mathbf{B}$ fields crossed at arbitrary angles. The reflective symmetry of the EVDF with respect to the v_xv_z-plane is no longer assumed, thus, the cells in the region of $v_y<0$ cannot be omitted. The collision propagator is still unchanged. On the other hand, the quantification of the acceleration propagator would become much complicated for the change in the crossing angle between the cell boundary and the acceleration vector $\mathbf{a}$ because $\mathbf{a}$ becomes helical for emergence of the E_y component when $\mathbf{E}\not\perp\mathbf{B}$. In addition, more generally, the diffusion coefficient becomes a tensor [29], [30], [31]. Calculations of the components of the tensorial diffusion coefficient would require moments weighted by xy and yz as well as that weighted by xz in (66). We need to keep calculation results of $m^{\rm C}_{1,x}(\mathbf{v})$, $m^{\rm C}_{1,y}(\mathbf{v})$, and $m^{\rm C}_{1,z}(\mathbf{v})$ for succeeding calculations of $m^{\rm C}_{2,x}(\mathbf{v})$, $m^{\rm C}_{2,y}(\mathbf{v})$, $m^{\rm C}_{2,z}(\mathbf{v})$, $m^{\rm C}_{2,xy}(\mathbf{v})$, $m^{\rm C}_{2,xz}(\mathbf{v})$, and $m^{\rm C}_{2,yz}(\mathbf{v})$. This requires a larger memory capacity.

Another extension would be calculations of higher-order moments for composition of the spatial electron distribution $f(\mathbf{r},\mathbf{v},t)$ under the $\mathbf{E}\times\mathbf{B}$ fields by using Hermite polynomials weighted by $m^{\rm L}_{n,r}(\mathbf{v},t)$. An effort to compose $f(x,\mathbf{v},t)$ in a one-dimensional model under a dc $\mathbf{E}$ field without $\mathbf{B}$ field calculated $m^{\rm L}_{n,x}(\mathbf{v},t)$ up to $n=9$ [15]. However, higher-order calculations under the $\mathbf{E}\times\mathbf{B}$ fields would possibly involve issues such as accumulation of numerical errors, memory shortage, and heavy computational load. They currently seem to be of an only theoretical possibility.

D. Remarks for future investigation

In the present work, SF_6 was chosen for the test gas in order to confirm the fundamental performance of the PM under $\mathbf{E} \times \mathbf{B}$ fields in both ionization-dominated and attachment-dominated cases. However, some other gases can be considered as possible media in succeeding work for improvement of precision and extension of calculation conditions. The model gases introduced in Refs. [32] and [33] have often been used for benchmarks of electron swarm simulations under dc electric fields (e.g., Refs. [30] and [34]) and $\mathbf{E} \times \mathbf{B}$ fields (e.g., Refs. [28] and [31]). They would be applicable for fine comparisons.

Data of the direction-dependent diffusion coefficients under $\mathbf{E}$ and $\mathbf{B}$ fields crossed at arbitrary angles are available for CF_4 [35] and a model gas [36]. Whether the negative differential conductivity [35] appears or not in each drift velocity component under $\mathbf{E} \times \mathbf{B}$ fields is also a point of interest.

When the PM calculation is applied to temporal, or furthermore, spatio-temporal development of electron swarms under $\mathbf{E} \times \mathbf{B}$ fields, behavior of the drift velocity components in temporarily varying crossed $\mathbf{E}$ and $\mathbf{B}$ fields seen in Ref. [35] can be a reference. Reproducibility of the transiently negative diffusion coefficients under crossed $\mathbf{E}$ and $\mathbf{B}$ fields [37] after stepwise change of $\mathbf{E}$ and $\mathbf{B}$ fields would also be a good viewpoint to examine the PM calculation.

VI. Conclusions

A PM technique to calculate real-space electron transport coefficients under $\mathbf{E}$ and $\mathbf{B}$ fields crossed at a right angle was developed. The centroid drift velocity vector and diffusion coefficients defined separately for the directions of $\mathbf{E}$, $\mathbf{B}$, and $\mathbf{E} \times \mathbf{B}$ were calculated by the PM applied to simultaneous moment equations derived from the BE. The results agreed with those calculated by MC simulations with discrepancies about a few percent.

The relaxation scheme previously applied to the EVDF worked successfully also in the relaxation of the first- and second-order moment distribution functions. However, in order to improve the convergence speed and precision of the PM, it would be necessary to systematically investigate their dependence on various factors such as the resolution of the cell partitioning and the relaxation scheme.

Nonetheless, a prototype of the PM calculation scheme for the real-space electron transport coefficients under $\mathbf{E}$ and $\mathbf{B}$ fields has been established. In addition to MC simulations, the PM has become a choice in the derivation of a set of electron transport coefficients for fluid model simulations of magnetized plasmas. The deterministic calculation scheme of the PM would be an advantage in some conditions severe for the MC simulations such as strong $\mathbf{B}$ fields and low $\mathbf{E}$ fields under which the electron population decreases for attachment during a long relaxation period. It is expected that further numerical efforts, e.g., customization of the relaxation scheme and implementation of the PM to parallel processing computers, would lead to higher performance of the PM in practical calculations.

Acknowledgement

This work was supported by a KAKENHI grant JP16K05626 from the Japan Society for the Promotion of Science.

References

[1] I. Adamovich, S. D. Baalrud, A. Bogaerts, P. J. Bruggeman, M. Cappelli, V. Colombo, U. Czarnetzki, U. Ebert, J. G. Eden, P. Favia, D. B. Graves, S. Hamaguchi, G. Hieftje, M. Hori, I. D. Kaganovich, U. Kortshagen, M. J. Kushner, N. J. Mason, S. Mazouffre, S. Mededovic Thagard, H.-R. Metelmann, A. Mizuno, E. Moreau, A. B. Murphy, B. A. Niemira, G. S. Oehrlein, Z. Lj. Petrovic, L. C. Pitchford, Y.-K. Pu, S. Rauf, O. Sakai, S. Samukawa, S. Starikovskaia, J. Tennyson, K. Terashima, M. M. Turner, M. C. M. van de Sanden, and A. Vardelle, "The 2017 plasma roadmap: low temperature plasma science and technology," J. Phys. D: Appl. Phys., vol. 50, no. 32, 323001 (46 pp.), July 2017, doi: 10.1088/1361-6463/aa76f5.

[2] P. J. Bruggeman, M. J. Kushner, B. R. Locke, J. G. E. Gardeniers, W. G. Graham, D. B. Graves, R. C. H. M. Hofman-Caris, D. Maric, J. P. Reid, E. Ceriani, D. Fernandez Rivas, J. E. Foster, S. C. Garrick, Y. Gorbanev, S. Hamaguchi, F. Iza, H. Jablonowski, E. Klimova, J. Kolb, F. Krcma, P. Lukes, Z. Machala, I. Marinov, D. Mariotti, S. Mededovic Thagard, D. Minakata, E. C. Neyts, J. Pawlat, Z. Lj. Petrovic, R. Pflieger, S. Reuter, D. C. Schram, S. Schröter, M. Shiraiwa, B. Tarabová, P. A. Tsai, J. R. R. Verlet, T. von Woedtke, K. R. Wilson, K. Yasui and G. Zvereva, "Plasma–liquid interactions: a review and roadmap," Plasma Sources Sci. Technol., vol. 25, no. 5, 053002 (59 pp.), September 2016, doi: 10.1088/0963-0252/25/5/053002.

[3] H. Sugawara, "A relaxation-accelerated propagator method for calculations of electron energy distribution function and electron transport parameters in gas under dc electric fields," Plasma Sources Sci. Technol., vol. 26, no. 4, 044002 (16 pp.), March 2017, doi: 10.1088/1361-6595/aa5d7f.

[4] P. J. Drallos and J. M. Wadehra, "A novel algorithm for calculating the time evolution of the electron energy distribution function in gaseous discharge," J. Appl. Phys., vol. 63, no. 11, pp. 5601–5603, June 1988, doi: 10.1063/1.340340.

[5] P. J. Drallos and J. M. Wadehra, "Exact time-dependent evolution of electron-velocity distribution functions in a gas using the Boltzmann equation," Phys. Rev. A, vol. 40, no. 4, pp. 1967–1975, August 1989, doi: 10.1103/PhysRevA.40.1967.

[6] T. J. Sommerer, W. N. G. Hitchon, and J. E. Lawler, "Self-consistent kinetic model of the cathode fall of a glow discharge," Phys. Rev. A, vol. 39, no. 12, pp. 6356–6366, June 1989, doi: 10.1103/PhysRevA.39.6356.

[7] H. Sugawara, Y. Sakai, and H. Tagashira, "Position-dependent electron swarm behaviour in steady-state Townsend discharges," J. Phys. D: Appl. Phys., vol. 25, no. 10, pp. 1483–1487, October 1992, doi: 10.1088/0022-3727/25/10/013.

[8] H. Sugawara, Y. Sakai, and H. Tagashira, "Analyses of electron swarms in gases in steady-state Townsend conditions," J. Phys. D: Appl. Phys., vol. 27, no. 1, pp. 90–94, January 1994, doi: 10.1088/0022-3727/27/1/013.

[9] H. Sugawara, Y. Sakai, and H. Tagashira, "Properties of electron swarms in gases in the upstream region of an electron source," J. Phys. D: Appl. Phys., vol. 28, no. 1, pp. 61–67, January 1995, doi: 10.1088/0022-3727/28/1/011.

[10] T. J. Sommerer, W. N. G. Hitchon, R. E. P. Harvey, and J. E. Lawler, "Self-consistent kinetic calculations of helium rf glow discharges," Phys. Rev. A, vol. 43, no. 8, pp. 4452–4472, April 1991, doi: 10.1103/PhysRevA.43.4452.

[11] K. Maeda and T. Makabe, "Time-dependent rf swarm transport by direct numerical procedure of the Boltzmann equation," Japan. J. Appl. Phys., vol. 33, no. 7B, pp. 4173–4176, July 1994, doi: 10.1143/JJAP.33.4173.

[12] T. Shimada, Y. Nakamura, Z. Lj. Petrović, and T. Makabe, "Electron transport coefficients in SiH_4 and Si_2H_6 in dc and rf fields," J. Phys. D: Appl. Phys., vol. 36, no. 16, pp. 1936–1946, August 2003, doi: 10.1088/0022-3727/36/16/304.

[13] H. Sugawara and Y. Sakai, "Electron acceleration in gas by impulse electric field and its application to selective promotion of an electron-molecule reaction," J. Phys. D: Appl. Phys., vol. 36, no. 16, pp. 1994–2000, August 2003, doi: 10.1088/0022-3727/36/16/311.

[14] H. Sugawara, H. Tagashira, and Y. Sakai, "Evaluation of real space electron drift velocity in gases using moment equations performed in velocity space," J. Phys. D: Appl. Phys., vol. 30, no. 3, pp. 368–373, February 1997, doi: 10.1088/0022-3727/30/3/009.

[15] H. Sugawara, Y. Sakai, H. Tagashira, and K. Kitamori, "The spatio-temporal development of electron swarms in gases: moment equation analysis and Hermite polynomial expansion," J. Phys. D: Appl. Phys., vol. 31, no. 3, pp. 319–327, February 1998, doi: 10.1088/0022-3727/31/3/011.

[16] H. Sugawara and Y. Sakai, "An analysis of transverse evolution of electron swarms in gases using moment equations and a propagator method," J. Phys. D: Appl. Phys., vol. 32, no. 14, pp. 1671–1680, July 1999, doi: 10.1088/0022-3727/32/14/320.

[17] H. Sugawara and Y. Sakai, "Equality of the higher-order diffusion coefficients between component and composite electron swarms in gas," Japan. J. Appl. Phys., vol. 45, no. 6A, pp. 5189–5196, June 2006, doi: 10.1143/JJAP.45.5189.

[18] H. Sugawara, "Calculation of electron velocity distribution function under crossed electric and magnetic fields using a propagator method," presented at the *33rd Int. Conf. Phenomena in Ionized Gases*, PI-6, Estoril, Lisboa, Portugal, July 9–14, 2017.

[19] H. Sugawara, "Calculation of real-space electron transport coefficients under crossed electric and magnetic fields by a propagator method," presented at the *10th Asia-Pacific Int. Symp. on the Basics and Applications of Plasma Technol.*, S3-01, Taoyuan, Taiwan, December 15–17, 2017.

[20] S. Dujko, Z. M. Raspopović, and Z. Lj. Petrović, "Monte Carlo studies of electron transport in crossed electric and magnetic fields in CF_4," J. Phys. D: Appl. Phys., vol. 38, no. 16, pp. 2952–2966, August 2005, doi: 10.1088/0022-3727/38/16/032.

[21] H. Sugawara, T. Yahata, A. Oda, and Y. Sakai, "The drift velocity vector of electron swarms in crossed electric and magnetic fields," J. Phys. D: Appl. Phys., vol. 33, no. 10, pp. 1191–1196, May 2000, doi: 10.1088/0022-3727/33/10/309.

[22] H. Tagashira, Y. Sakai, and S. Sakamoto, "The development of electron avalanches in argon at high E/N values: II. Boltzmann equation analysis," J. Phys. D: Appl. Phys., vol. 10, no. 7, pp. 1051–1063, May 1977, doi: 10.1088/0022-3727/10/7/011.

[23] R. E. Robson, "Transport phenomena in the presence of reactions: definition and measurement of transport coefficients," Aust. J. Phys., vol. 44, no. 6, pp. 685–692, 1991, doi: 10.1071/PH910685.

[24] H. Itoh, T. Matsumura, K. Satoh, H. Date, Y. Nakao, and H. Tagashira, "Electron transport coefficients in SF_6," J. Phys. D: Appl. Phys., vol. 26, no. 11, pp. 1975–1979, November 1993, doi: 10.1088/0022-3727/26/11/020.

[25] H. Itoh, Y. Miura, N. Ikuta, Y. Nakao, and H. Tagashira, "Electron swarm development in SF_6: I. Boltzmann-equation analysis," J. Phys. D: Appl. Phys., vol. 21, no. 6, pp. 922–930, June 1988, doi: 10.1088/0022-3727/21/6/010.

[26] J. Mirić, D. Bošnjaković, I. Simonović, Z. Lj. Petrović, and S. Dujko, "Electron swarm properties under the influence of a very strong attachment in SF_6 and CF_3I obtained by Monte Carlo rescaling procedures," Plasma Sources Sci. Technol., vol. 25, no. 6, 065010 (15 pp.), December 2016, doi: 10.1088/0963-0252/25/6/065010.

[27] H. Sugawara, "Efficiency and limitation of periodic sample multiplication to reduce computational load in Monte Carlo simulations of electron swarms in gas under attachment-dominated conditions," Japan. J. Appl. Phys., vol. 57, no. 3, 038001 (3 pp.), January 2018, doi: 10.7567/JJAP.57.038001.

[28] R. D. White, M. J. Brennan, and K. F. Ness, "Benchmark simulations for electron swarms in crossed electric and magnetic fields," J. Phys. D: Appl. Phys., vol. 30, no. 5, pp. 810–816, March 1997, doi: 10.1088/0022-3727/30/5/014.

[29] R. D. White, K. F. Ness, R. E. Robson, and B. Li, "Charged-particle transport in gases in electric and magnetic fields crossed at arbitrary angles: multiterm solution of Boltzmann's equation," Phys. Rev. E, vol. 60, no. 2, pp. 2231–2249, August 1999, doi: 10.1103/PhysRevE.60.2231.

[30] A. M. Nolan, M. J. Brennan, K. F. Ness, and A. B. Wedding, "A benchmark model for analysis of electron transport in non-conservative gases," J. Phys D: Appl. Phys. vol. 30, no. 20, pp. 2865–2871, October 1997, doi: 10.1088/0022-3727/30/20/013.

[31] Z. Raspopović, S. Sakadžić, S. A. Bzenić, and Z. Lj. Petrović, "Benchmark calculations for Monte Carlo simulations of electron transport," IEEE Trans. Plasma Sci., vol. 27, no. 5, pp. 1241–1248, October 1999, doi: 10.1109/27.799799.

[32] J. Lucas and H. T. Saelee, "A comparison of a Monte Carlo simulation and the Boltzmann solution for electron swarm motion in gases," J. Phys. D: Appl. Phys., vol. 8, no. 6, pp. 640–650, April 1975, doi: 10.1088/0022-3727/8/6/007.

[33] I. D. Reid, "Investigation of the accuracy of numerical-solutions of Boltzmann-equation for electron swarms in gases with large inelastic cross-sections," Aust. J. Phys., vol. 32, no. 3, pp. 231–254, 1979, doi: 10.1071/PH790231.

[34] K. F. Ness and R. E. Robson, "Velocity distribution function and transport coefficients of electron swarms in gases. II. Moment equations and applications," Phys. Rev. A, vol. 34, no. 3, pp. 2185–2209, September 1986, doi: 10.1103/PhysRevA.34.2185.

[35] Z. Lj. Petrović, S. Dujko, D. Marić, G. Malović,Ž. Nikitović, O. Šašić, J. Jovanović, V. Stojanović, and M. Radmilović-Radjenović, "Measurement and interpretation of swarm parameters and their application in plasma modelling," J. Phys. D: Appl. Phys., vol. 42, no. 19, 194002 (33 pp.), September 2009, doi: 10.1088/0022-3727/42/19/194002.

[36] S. Dujko, R. D. White, Z. Lj. Petrović, and R. E. Robson, "Benchmark calculations of nonconservative charged-particle swarms in dc electric and magnetic fields crossed at arbitrary angles," Phys. Rev. E, vol. 81, no. 4, 046403 (18 pp.), April 2010, doi: 10.1103/PhysRevE.81.046403.

[37] R. D. White, S. Dujko, K. F. Ness, R. E. Robson, Z. Raspopović, Z. Lj. Petrović, "On the existence of transiently negative diffusion coefficients for electrons in gases in E x B fields," J. Phys. D: Appl. Phys., vol. 41, no. 2, 025206 (7 pp.), January 2008, doi: 10.1088/0022-3727/41/2/025206.

PLACE PHOTO HERE

Hirotake Sugawara was born in Japan in 1967. He received the B.E., M.E., and D.E. degrees in electrical engineering from Hokkaido University, Sapporo, Japan, in 1990, 1992, and 1997, respectively.

From 1992 to 1998, he was a Research Associate with the Department of Electrical Engineering, Hokkaido University, where he was an Associate Professor in 1998. He is currently an Associate Professor with the Division of Electronics for Informatics, Graduate School of Information Science and Technology, Hokkaido University.

Dr. Sugawara is a senior member of the IEE of Japan and a member of Japan Society of Applied Physics.